Microwave transmission modes in compound metallic gratings

Y. G. Ma,[1,*] X. S. Rao,[2] G. F. Zhang,[1] and C. K. Ong[1]
[1]*Centre for Superconducting and Magnetic Materials, Department of Physics, National University of Singapore, Singapore 117542, Singapore*
[2]*Temasek Laboratories, National University of Singapore, Singapore 119260, Singapore*
(Received 4 April 2007; revised manuscript received 10 May 2007; published 10 August 2007)

Microwave transmission through one-dimensional metallic compound grating is studied up to 18 GHz. The metallic compound grating consists of a basic unit of one slit (*a* type), two slits (*ab* type), and three slits (*abc* type) of different widths. Greatly enhanced transmission is observed at the frequencies near the first and second order waveguide harmonics. The splitting of transmission peak is found for the *ab*- and *abc*-type grating. This effect is explained by the multiphase patterns of the *E*-field distributions inside the slits, predicted by the numerical calculations. These resonance modes are further physically understood in terms of their photonic band structures. The theoretical bands for the *a*-type grating are calculated using a quasianalytic model and those for the *ab*- and *abc*-type gratings with superlattice periodicities are plotted according to Brillouin zone folding effect, which show good agreement with the measured results.

DOI: 10.1103/PhysRevB.76.085413 PACS number(s): 73.20.Mf, 78.70.Gq, 42.25.Bs, 42.79.Dj

I. INTRODUCTION

In the last few years after the discovery of extraordinary light transmission through two-dimensional metallic hole arrays,[1] a great deal of effort has been done to understand the electromagnetic (EM) diffraction through subwavelength metallic apertures triggered by both scientific interests and potential important applications.[2–4] So far, the excitation of surface plasmon polaritons (SPPs) in the dielectric/metal interface[5–8] has been generally believed to play a crucial role in this effect. In one-dimensional metallic grating, the localized cavity and/or slit field resonance, regarded as waveguide mode, can also give rise to enhanced electromagnetic transmission or absorption.[9] Other than the SPPs and waveguide mode, there is a third kind of resonance, known as phase resonance,[10,11] reported in metallic gratings with period of several cavities and/or slits contributed to the enhancement of the transmission mode. For such compound gratings, when illuminated at *p*-polarized radiation there are characteristic frequencies at which the adjacent slits can resonate at out-of-phase configurations accompanied by strong field intensification effect inside the cavity and/or slit.[12,13] The increase of the cavity and/or slit numbers in compound gratings will give rise to new degrees of freedom for the near-field distribution. The multiple patterns for phase resonance can be produced as a result of redistribution of electromagnetic energies when reaching the characteristic frequencies at different diffraction orders. A resultant maximization of the specular efficiency or splitting of transmission peak has been predicted in compound gratings of finite arrays of cavities and/or slits in period.[13–15]

In this work, we study the microwave transmissions on compound metallic gratings. Their structures are changed by periodically increasing the slit widths in the Al slat arrays. Different from the previously reported gratings,[14,15] our compound gratings are of no structural symmetry in their basic units. Thus, they can be regarded as the general cases for electromagnetic diffractions on metallic gratings and can excite all the possible resonance modes at normal incidence without degeneracy. Complex transmission features (peak and dip) associated with these resonance modes are observed, which are numerically understood[16] by multiphase distributions of the resonant fields inside the slits. The physical origin for these phase patterns is explored in terms of their photonic band structures from both experimental measurement and theoretical calculations where a quasianalytic model and Brillouin zone folding effect are employed.

II. SAMPLES AND MEASUREMENT

In Fig. 1, we schematically show the samples constructed by stacking together 30 aluminum slats of width $w=4.5$ mm, height $h=18.5$ mm, and length ~30 cm. Figure 1(a) shows the structure of a uniform grating with air-filled slit of width $a=0.5$ mm, thereby corresponding to a period $d=5$ mm. Figures 1(b) and 1(c) show two compound gratings with unit cells consisting of two slits (of widths $a=0.25$ mm and $b=0.5$ mm) and three slits (of widths a

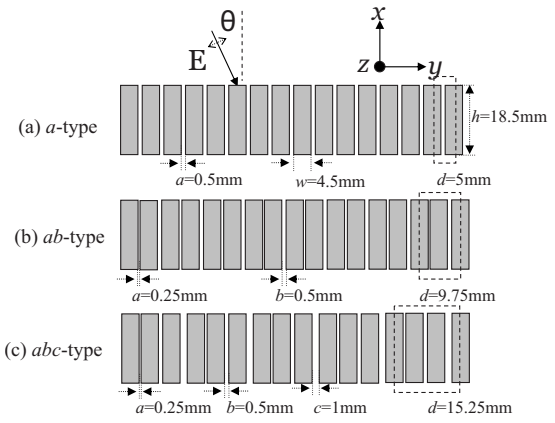

FIG. 1. Schematic illustrations of the sample gratings of (a) *a* type, (b) *ab* type, and (c) *abc* type together with their parameters. The incidence plane is in the *yz* plane with the *E*-field directions perpendicular to the grating slits.

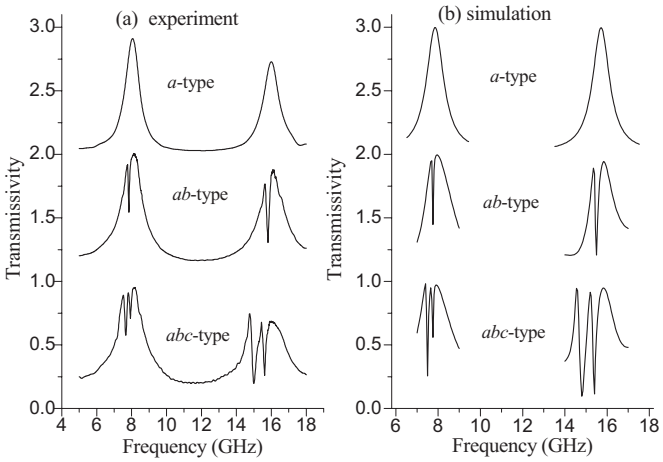

FIG. 2. (a) Measured transmission spectra of the samples given in Fig. 1 together with (b) the results predicted from the numerical simulations. For the sake of clarity, the transmissivities of the *a*- and *ab*-type gratings are, respectively, upward moved by 2 and 1.

=0.25 mm, b=0.5 mm, and c=1 mm), respectively giving periods of d=9.75 and 15.25 mm. Here, we denote the three gratings by *a*-, *ab*-, and *abc*-type gratings according to the slit width's distributions in their basic units. Microwave absorption foams are placed around the samples to reduce the side scattering or leaking. The microwave signals are produced and dealt by a vector network analyzer (HP 8722) with frequency band from 5 to 18 GHz. *p*-polarized (TM mode) plane waves from a transmitting horn are radiated upon the gratings with the incidence plane (in the *yz* plane) perpendicular to the grating slits. The transmitted signals are collected by a receiving horn. The horn-to-sample distance along their coaxis is fixed at 30 cm.

III. TRANSMISSION SPECTRA

Figure 2(a) gives the experimental transmission spectra from the samples shown in Fig. 1 illuminated at normal incidence together with the simulated transmission spectra in Fig. 2(b). For the *a*-type grating, there are two resonant peaks, centered at 8.06 and 16 GHz in its spectrum as shown in Fig. 2(a). These two resonant peaks also appear in the *ab*- and *abc*-type gratings. For the *ab*-type grating, a transmissivity dip in the left wing of one primary mode is observed, and two dips appear for the *abc*-type grating. The numerical simulations in Fig. 2(b) could reproduce the transmission spectra obtained from the experiments. The small frequency shifts ($<$0.1 GHz) and the amplitude differences might be caused by two reasons: one is confined by the near-field measurement method by which the incident waves are only pseudo plane waves, and the other is the existence of structural fluctuations within the samples (such as slat dimensions or their spacing).

The enhanced transmission on metallic gratings can be realized with the excitation of SPP-like surface wave resonance and/or waveguide resonance. For the *a*-type grating under normal microwave radiation, the first order SPP-like mode can be predicted at a wavelength near the grating period of 5 mm. It corresponds to a resonance frequency of 60 GHz, far beyond our measuring frequency range. So the SPP-like resonance can be excluded in considering the physical modes responsible for the transmission peaks. In the ideal case of perfect conductivity and infinitesimal slit width, waveguide resonance can be regarded as a Fabry-Pérot-like mode with their resonant frequencies $f=Nc/2h$ (here c is the light velocity in vacuum, h is the grating height, and N is the resonant order). Let h=18.5 mm in this case. The predicted resonant frequencies for the first (N=1) and second (N=2) order harmonic are 8.11 and 16.22 GHz, very close to the above measured values. Thus, these two resonance peaks could be attributed to the first and second order waveguide harmonics. For the *ab*- or *abc*-type grating, this primary waveguide mode does not change but new orders should be introduced, which are responsible for the splitting of transmission peaks.

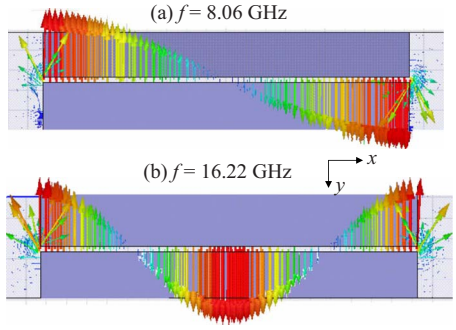

FIG. 3. (Color online) Prediction of the *E*-field distributions (in the *xy* plane) at normal incidence for the *a*-type grating at the frequencies corresponding to (a) the first waveguide harmonic (8.06 GHz) and (b) the second harmonic (16.22 GHz). The amplitude of the field is indicated by the length of the arrow.

IV. ELECTRIC FIELD CONFIGURATIONS

The underlying diffraction processes for these transmission features can be drawn from the numerically calculated electric field patterns. Figures 3(a) and 3(b) give the calculated *E*-field distributions for the *a*-type grating at the first (8.06 GHz) and second order (16.22 GHz) waveguide harmonics. Standing waves with strong intensities are observed inside the slits, while the waves localized on the grating surface are very weak. These intensified slit fields will be forward propagated and constructively interfered out of the gratings, consequently giving rise to the greatly enhanced transmission efficiency with the slit width far smaller than the grating period and the incident wavelength.

Figure 4 gives the *E*-field distributions for the *ab*-type grating at the frequencies corresponding to (a) the first peak (15.35 GHz), (b) the dip (15.5 GHz), and (c) the second peak (15.85 GHz) on the second order waveguide harmonic. As shown in Fig. 4(a), the fields in the two slits have opposite resonant directions, suggesting an out-of-phase configuration by π radian phase difference, i.e., the so-called phase resonance.[10,11] Such a phase pattern can also be described by "+ −" following the terminology of Ref. 15, where "+" and

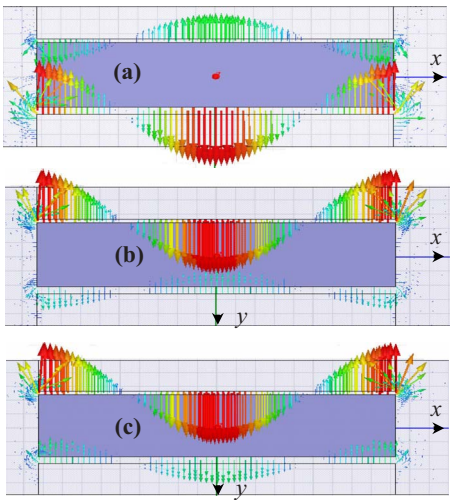

FIG. 4. (Color online) Prediction of the *E*-field distributions (in the *xy* plane) at normal incidence for the *ab*-type grating at the frequencies corresponding to (a) the first peak (15.35 GHz), (b) the dip (15.5 GHz), and (c) the second peak (15.85 GHz) on the second waveguide harmonic. The amplitude of the field is indicated by the length of the arrow. The slit fields in (a) and (b) correspond to the out-of-phase pattern ("+ −") and that in (c) corresponds to the in-phase pattern ("+ +"). The redistribution of the field intensities in the slits on increasing the resonant frequency is manifest.

"−" represent the slit fields of zero and π radian phase difference with the incident fields, respectively. The far transmitted EM fields are the interfered result of the fields, emitted from both slits, while the emission efficiency is proportional to the product of the energy flux ($\propto$ resonant field intensity) and the emission area ($\propto$ slit width). At this frequency, the resonant field in the wider slit (b=0.5 mm) is much stronger in intensity than that in the narrower slit (a =0.25 mm) and thus the former will have much larger energy flux flowing through its emission end and dominate the total transmission efficiency by also a larger emission area. It gives the first transmission peak at its maximum resonant state. In Fig. 4(b), these two slits are still in the out-of-phase configuration but the stronger resonant state shifts into the narrower slit. At this frequency, the energy flux through the emission end of the wider slit is smaller than that at the narrower slit but its product with the emission area will give the two slits comparable EM emission efficiencies. The far EM fields emitted from these two slit ends will be destructively interfered and thus give a transmission dip at this frequency. For the case in Fig. 4(c), the phase configuration for the two slits returns into the in-phase pattern ("+ +") and then the emitted fields will be enhanced again by constructive interference. Thus, a second transmission peak is observed. Close inspection on the *E*-field patterns at different frequencies shows that the out-of-phase configuration exists only in a narrow frequency region near the dip.

For the *abc*-type grating, one primary waveguide harmonic consists of three peaks and two dips (see Fig. 2). Three possible phase configurations for the three slits are supported in this case. These correspond to two out-of-phase patterns of "+ + −" around the first dip and "+ − −" around the second dip, and the in-phase pattern of "+ + +" in the rest of the frequency bands within one primary resonance peak. The field configurations in the slits at each transmission peak or dip in the second order harmonic are further illustrated and simply described by a number of arrows, as tabulated in Table I where the "upward" arrows mean in phase with the incident field and the numbers of arrows denote the relative intensities of the resonant fields in each slit. The narrowest slit (0.25 mm) always keeps in phase with the incident field, while the other two vary with the resonant frequency. The stronger resonant field tends to move into the narrower slit when the resonant frequency increases. The redistribution of the field intensity among the slits directly leads to the peak-to-dip shifting on the transmission efficiency within one out-of-phase pattern, as discussed above on the *ab*-type grating.

TABLE I. Simplified illustration of the *E*-field distributions among the slits at the transmission peak or dip on the second order harmonic of the *abc*-type grating by arrows. The "upward" arrows mean in phase with the incident field and their numbers denote the relative intensities of the resonant fields among the slits.

Description	Frequency (GHz)	Field distributions in the slits		
		a (0.25 mm)	b (0.5 mm)	c (1 mm)
First peak	14.6	↑	↑↑	↓↓↓
First dip	14.9	↑	↑↑↑	↓↓
Second peak	15.25	↑↑	↓↓↓	↓
Second dip	15.4	↑↑↑	↓↓	↓
Third peak	15.8	↑↑↑	↑↑	↑

The frequency dependence of the resonant state for each slit could be understood by considering their finite widths. In the case of perfect conductivity and subwavelength slit width, the fundamental eigenmode in the modal expansion of the electric and magnetic fields inside the slits forms the propagating waves, while the high eigenmodes disappear evanescently at the slit ends.[17] Although having limit effect on the transmission efficiency, the high order components do broaden the resonant peaks and shift the characteristic resonant frequency to lower values when the slit width increases.[15,18] These effects make each slit in one period have its own characteristic frequency where the field intensity in the slit reaches maximum. These frequencies can be separately reached by scanning the external driving frequency. Therefore, there is a sequential redistribution of the field intensities among the slits. The sequence to excite the characteristic resonance in these slits plays a key role in forming the final resonant phase patterns. For the *abc*-type grating, the phase patterns within one harmonic will continuously change from "+ + −" to "+ − −" and last to "+ + +" when the characteristic resonance is sequentially excited from *c* slit to *b* slit and last to *a* slit on increasing the external driving frequency. There is no phase pattern of "+ − +" because the *a* and *c* slits cannot adjacently reach their characteristic resonance. To further verify this point, we rearrange the slit order in a different way to form a *bac*-type grating. In this case, the observed phase patterns are "+ + −", "− + −", and "+ + +". The pattern of

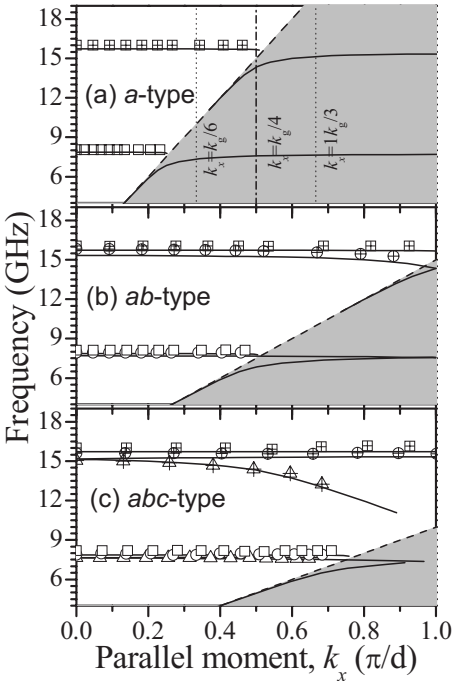

FIG. 5. The photonic band structures of the (a) *a*-type, (b) *ab*-type, and (c) *abc*-type gratings. The measured results represented by the squares, circles, and triangles are obtained from the transmission peaks on each harmonic. The theoretical bands denoted by the solid lines in (a) are calculated according to the method described in Ref. 9, while those in (b) and (c) are plotted by the simple symmetrical translation of the theoretical bands given in (a) in terms of Brillouin zone folding effect. The shaded area denotes the nonradiative region.

"+ − −" does not appear because the *a* slit and *c* slit cannot adjacently reach their characteristic resonant states, while the pattern of "− + −" appears because the characteristic resonance in the *b* and *c* slits can be adjacently excited.

V. PHOTONIC BAND STRUCTURES

It is seen that the multiphase configurations for the *E* fields in the slits play a crucial role in inducing the complex transmission features on the compound gratings. The physical origin for the phase resonance can be better understood from their photonic band structures. Here, we discuss it from both experimental measurement and a Brillouin zone folding approach. Figure 5 plots the energy band dispersions for the three type gratings as a function of the parallel wave vector (k_x). The experimental values (represented by the squares, circles and triangles) are from the local peaks on the transmission spectra obtained by gradually increasing the incident angle (θ) (where $k_x=\omega/c_0 \sin\theta$, c_0 is the light velocity). For the measured results, the *a*-type grating shows two flatbands located at ~8.0 and ~16.0 GHz, while the *ab*- and *abc*-type gratings have one and two more dispersions near either frequency. The bottom band near ~16.0 GHz for the *ab*- or *abc*-type grating shows a curved dispersion as the parallel momentum approaches the first Brillouin zone boundary ($k_g/2=\pi/d$).

For the *a*-type grating, in the limit of perfect conductivity and subwavelength slit width, a pseudoanalytic model can be used to study the microwave transmissions.[19,20] This model is based on the consideration of the surface-impedance boundary conditions on the metallic boundaries and the fundamental eigenmode in the modal expansion of the electromagnetic field inside the slits. As discussed in Ref. 9, in this case, the field amplitudes inside the slit are proportional to a factor of $1/D$, where the denominator D is given by

$$D=[1-(1+\eta)\psi]^2 e^{ik_0 h}-[1+(1-\eta)\psi]^2 e^{-ik_0 h}, \qquad (1)$$

with the surface impedance $\eta=(\varepsilon_{\text{metal}})^{-1/2}$ and the function ψ in the form of

$$\psi=\frac{a}{d}\sum_{m=-\infty}^{\infty}\frac{\left[\sin c\left(\frac{k_0\gamma_m a}{2}\right)\right]^2}{(1-\gamma_m^2)^{1/2}+\eta}, \qquad (2)$$

where $\gamma_m=k_x/k_0+m\lambda/d$ is associated with the *m*th diffraction order, and $\text{sinc}\,\xi\equiv\sin\xi/\xi(\xi=k_0\gamma_m a/2)$ is the overlapping function between the *m*th order plane wave and the fundamental eigenmode inside the slit. It is found that there is a close correspondence between the maxima of transmittance and the spectra positions of the zeros of the imaginary part of D, and the photonic band structures for the *a*-type grating can be obtained by studying this zero condition.[9] The calculated bands are shown in Fig. 5(a) denoted by the solid lines, which comprised four components up to 18 GHz: two flatbands within the light cone and two curved parts outside the light cone (shaded area). The flatbands belong to the first and second order waveguide modes, which are typically independent of incident angles. For the nonradiative bands, they continuously transfer from the SPP mode to the waveguide mode, as evidenced by deviating from the incident light line ($\omega=c_0k_0$) and gradually approaching horizontal asymptotical lines on increasing the parallel wave vectors toward the first Brillouin zone boundary.[21] Therefore, the photonic band structure for the *a*-type grating is a combination of flatbands associated with waveguide resonance and bands with basically SPP character. It is worth commenting that the slit fields are strongly coupled with the surface waves, as defined by the overlapping function sinc ξ, so it is physically reasonable for the nonradiative bands to have continuous transition from the SPP mode to the waveguide mode.[22]

Structurally, the *a*-type grating has the lattice of single period, while the *ab*- or *abc*-type grating can be considered to have the lattice structures containing more than one periodicity that creates a superlattice periodicity.[23] The size of the real space unit for the compound gratings will be increased, which will decrease the size of the first Brillouin zone. In the process, additional photonic bands will be created via the Brillouin zone folding effect.[24] Compared to the *a*-type grating, the *ab*- and *abc*-type superlattice structures have two and three times increase in their unit sizes, which decrease the sizes of their first Brillouin zones by the same times. As a result, for the *ab*-type grating, the photonic bands from $k_g/4$ to $k_g/2$ in Fig. 5(a) will be folded back into the first half region by projecting along the symmetrical axis at $k_x=k_g/4$ (the dash dot line). Therefore, one more band just

below each original flatband appears, as shown in Fig. 5(b). For the *abc*-type grating, the two portions from $k_g/6$ to $k_g/3$ and from $k_g/3$ to $k_g/2$ on the bands in Fig. 5(a) will be folded back and two more bands below each original flatband are formed in the new first Brillouin zone, as shown in Fig. 5(c). In Figs. 5(b) and 5(c), it can be seen that the predicted band dispersions obtained by simple symmetric translations are in good agreement with the measuring results except for the small data drifting in the *y* axis. The different energy levels of these bands will give rise to different electromagnetic field distributions on the compound gratings, which are manifested by the multiple phase patterns for the *E* fields localized inside the slits as numerically predicted above.

The photonic band structures of the compound gratings are found to be closely dependent on their unit structures. We measured the transmission spectrum (not shown here) of an *aba*-type grating ($a=0.5$ mm, $b=1.0$ mm, $h=18.5$ mm) and only found two photonic bands corresponding to the slit field patterns of "+ − +" and "+ + +" near each waveguide harmonic at low incident angles. This is because the other possible band with phase difference between the two *a* slits in one unit (such as phase pattern "+ + −") is symmetrically confined at low incident angles.[14,25] In this case, the subband degeneracy might have happened due to the structural symmetry. For the *abc*-type grating, there is no such symmetric confinement that all the possible bands should be observable without degeneracy. This validates the discussion of its band diagram by the Brillouin zone folding approach. We also extend this approach to the case of an *abcd*-type grating where four bands near each waveguide harmonic are expectedly observed by following the predictions from the four-time folding of the first Brillouin zone of the *a*-type grating. Lastly, it should be emphasized that the folding procedure used here to generate the band diagram is an approximate method, which is only applicable to the gratings of no structural symmetry and invalid for the symmetrical gratings. For the latter, the correct picture for the band diagram should be given by a more rigorous method, as has already been done by Skigin and Depine using transfer matrix formalism (see Fig. 4 in Ref. 25). Their numerical results showed that there was no direct correlation between the numbers of the subbands near one waveguide harmonic and the slit in one unit for the symmetrical gratings, and some bands corresponding to certain phase configurations inside the slits would be inhibited by the symmetry requirement at normal incidence but really appear at oblique illumination where the symmetry condition was removed, which is in good agreement with the previous experimental results for an *aba*-type grating (see Fig. 4 in Ref. 14).

VI. CONCLUSIONS

We have showed that greatly enhanced transmission efficiency on metallic gratings could be obtained by exciting the waveguide resonance. The transmission features become more complex with peak splitting on compound gratings where superlattice periodicity is introduced. Numerical calculations show that these complex features are induced by the out-of-phase resonance for the electric fields localized inside the slits on the compound gratings. The physical origin for these phase resonance modes is discussed in terms of their photonic band structures. The band folding effect has been established to interpret the measuring results, which show good agreement with the theoretical predictions. Our experiments show that a different kind of microwave devices, such as frequency selector or filter, might be suggested by using compound metallic gratings.

*phymy@nus.edu.sg

[1] T. W. Ebbesen, H. J. Lezec, H. F. Ghaemi, T. Thio, and P. A. Wolff, Nature (London) **391**, 667 (1998).
[2] B. Hou, Z. Hang, W. J. Wen, C. T. Chan, and P. Sheng, Appl. Phys. Lett. **89**, 131917 (2006).
[3] C. Genet and T. W. Ebbesen, Nature (London) **445**, 39 (2007).
[4] X. S. Rao and C. K. Ong, Phys. Rev. B **68**, 113103 (2003); Phys. Rev. E **68**, 067601 (2003).
[5] W. L. Barnes, A. Dereux, and T. W. Ebbesen, Nature (London) **424**, 824 (2003).
[6] L. Yin, V. K. Vlasko-Vlasov, A. Rydh, J. Pearson, U. Welp, S. H. Chang, S. K. Gray, G. C. Schatz, D. B. Brown, and C. W. Kimball, Appl. Phys. Lett. **85**, 467 (2004).
[7] P. Lalanne and J. P. Hugonin, Nature (London) **2**, 551 (2006).
[8] J. B. Pendry, L. Martin-Moreno, and F. J. Garcia-Vidal, Science **305**, 847 (2004).
[9] J. A. Porto, F. J. Garcia-Vidal, and J. B. Pendry, Phys. Rev. Lett. **83**, 2845 (1999).
[10] D. C. Skigin, V. V. Veremey, and R. Mittra, IEEE Trans. Antennas Propag. **47**, 376 (1999).
[11] D. C. Skigin, A. N. Fantino, and S. I. Grosz, J. Opt. A, Pure Appl. Opt. **5**, s129 (2003).
[12] D. C. Skigin and R. A. Depine, Opt. Commun. **262**, 270 (2006).
[13] A. N. Fantino, S. I. Grosz, and D. C. Skigin, Phys. Rev. E **64**, 016605 (2001).
[14] A. P. Hibbins, I. R. Hooper, M. J. Lockyear, and J. R. Sambles, Phys. Rev. Lett. **96**, 257402 (2006).
[15] D. C. Skigin and R. A. Depine, Phys. Rev. Lett. **95**, 217402 (2005).
[16] Finite element method computer modeling is done with the use of HFSS, Ansoft Corporation, Pittsburgh, PA.
[17] H. Lochbihler and R. Depine, Appl. Opt. **32**, 3459 (1993).
[18] Y. Takakura, Phys. Rev. Lett. **86**, 5601 (2001).
[19] P. Sheng, R. S. Stepleman, and P. N. Sanda, Phys. Rev. B **26**, 2907 (1982).
[20] F. J. Garcia-Vidal and L. Martin-Moreno, Phys. Rev. B **66**, 155412 (2002).
[21] W. C. Tan, T. W. Preist, J. R. Sambles, and N. P. Wanstall, Phys. Rev. B **59**, 12661 (1999).
[22] S. Collin, F. Pardo, R. Teissier, and J. L. Pelouard, Phys. Rev. B **63**, 033107 (2001).
[23] P. S. J. Russell, Phys. Rev. Lett. **56**, 596 (1986).
[24] C. W. Neff, T. Yamashita, and C. Summers, Appl. Phys. Lett. **90**, 021102 (2007).
[25] D. C. Skigin and R. A. Depine, Phys. Rev. E **74**, 046606 (2006).